Unsteady Flow Modeling of Helicopter Airfoils

Victor A. Anikin[1], Oleg V. Gerasimov[1], Boris S. Kritsky[2]

[1]Kamov Company
8 the 8th March Str. 140007 Lubertsy, Moscow Region, Russian Federation
e-mail: kb@kamov.ru

[2]Air Force Engineering Academy named after prof. N.E. Zhukovsky
3 Planetnaya Str., Moscow, 125190, Russian Federation
e-mail: kritsky@starlink.ru

Key words: Aerodynamics, modeling, airfoil, unsteady flow

Abstract: The mathematical model of unsteady flow of helicopter airfoils based on the model of separated flow around finite-thickness bodies of Belotserkovsky-Kotovsky-Nisht-Fedorov is addressed. The specific features of the model are as follows. Flow around a body is divided into two regions: viscous flow field in a boundary layer on a flow-immersed body and inviscid flow field outside the body and boundary layer on it. The flow in the latter field outside the vortex wake is assumed to be potential. With the body surface being smooth, the vortex wake behind the body can form only due to boundary-layer separation. In this case, the total vorticity of a boundary layer is carried off at separation points. Then the wake is modeled by free discrete vortices, whose circulation is defined by this vorticity.

Using the model, the integrated and distributed aerodynamic characteristics of helicopter airfoils, velocity fields and unsteady vortex wake can be calculated. The computational examples and comparison of computed results with experimental data are presented.

INTRODUCTION

The flows past rotor blade airfoils are known to be essentially unsteady even in steady horizontal flight. The blade sections executing complex curvilinear motions are situated in the varying-incidence flow conditions. In one rotor revolution, the Reynolds number of one and the same blade section varies through a wide range. The dimensionless blade load frequency , Strouhal number, also varies over a broad range. Rotor blade sections frequently operate in the near-stall and post-stall angle-of-attack ranges. Theoretical study of the three-dimensional separated flow about finite-thickness rotor blade is a rather complex problem requiring significant computational resources. To solve the helicopter rotor aerodynamic design problem and analyze its operation in flight conditions, especially in limiting regimes, it is reasonable, along with experimental investigations, to carry out numerical studies of flows about helicopter airfoils using cost-effective computational methods. Considered below is one of such methods for calculating aerodynamic characteristics of representative helicopter airfoils based on the model of separated flow about finite-thickness bodies presented in [1]. The model is founded on the synthesis of the models of inviscid incompressible flow and unsteady boundary layer flow. The numerical implementation of the model is based on the discrete vortex method for computing flow parameters in the inviscid flow region [2] and the method for computing unsteady boundary layers [3].

1. MATHEMATICAL MODEL

1.1 Problem formulation

The motion of the blade airfoil of a rotor having the translational velocity $\vec{U}_0$ is considered. Generally, together with the blade the airfoil may execute a complex motion caused by rotation about rotor axis, flap motion about flap hinge and rotation about feather hinge. The air velocity seen by the blade airfoil (Fig. 1) at an arbitrary point M_0 of its contour located at the relative radial distance $\vec{r}$ from the rotor axis is determined according to [4] as:

$$\vec{u}_0(M_0,t)=\vec{\vartheta}_{0x}(\bar{r},t)+\vec{\vartheta}_{0y}(\bar{r},t)+\vec{\vartheta}_{0\varphi}(M_0,t), \tag{1}$$

where $\vec{\vartheta}_{0x}$ is the air velocity component in the rotor rotation plane, $\vec{\vartheta}_{0y}$ is the air velocity component normal to the rotation plane, $\vec{\vartheta}_{0\varphi}$ is the air velocity component due to blade rotation about the feather hinge.

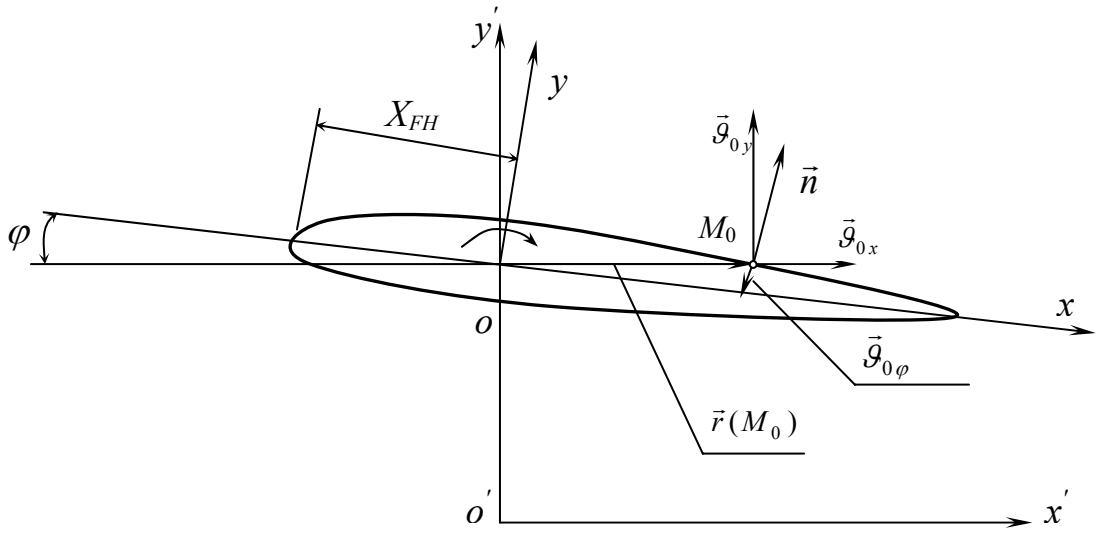

Figure 1. To the definition of motion kinematic parameters of a rotor blade section

The air velocity components entering into equation (1) are calculated as follows:

$$\vartheta_{0x}(\bar{r},t)=\bar{r}\cos\beta(t)+\bar{\vartheta}\cos\alpha\ \sin\psi(t), \tag{2}$$

$$\vartheta_{0y}(\bar{r},t)=\bar{\vartheta}\sin\alpha_{н}\cos\beta(t)+\bar{\vartheta}\cos\alpha_{н}\cos\psi(t)\sin\beta(t)+\bar{r}\omega_{\beta}(t), \tag{3}$$

$$\vartheta_{0\varphi}=\vec{\omega}_{FH}\times\vec{r}(M_0), \tag{4}$$

where β is the flapping angle, Ψ is the current blade azimuth angle, $\bar{\vartheta}$ is the relative rotor motion velocity, $\alpha_{н}$ is the rotor disk plane angle of attack, ω_{β} is the blade angular velocity about the flap hinge, $\vec{\omega}_{FH}$ is the blade angular velocity vector relative to the feather hinge, $\vec{r}$ is the position vector of a blade section contour point.

Thus, the motion of the blade airfoil can be considered generally as motion according to a polyharmonic law and, particularly, according to a harmonic law.

1.2 Numerical implementation

The flow about the blade airfoil section was divided into the two regions: the region of viscous flow in the boundary layer and the region of inviscid flow outside the boundary layer. In the latter region outside the vortex wake, the flow was assumed to be potential. The parameters of the inviscid flow were calculated by the discrete vortex method [2, 5]. Positioned on the airfoil contour therewith were the integrated discrete vortices replacing the bound and free vortices located on the airfoil. Arranged in the midway between the discrete vortices are the control points where the tangency boundary condition for the airfoil contour was met.

The components of disturbance velocity in the control point ν, induced by the integrated discrete vortices with the circulation $\Gamma_{\Sigma\mu}$, $\mu = 1,2,..., N$, and free vortices of the wake with the circulation δ_i, $i=1,2,..., K$, at a design instant of time r, were determined in the form:

$$w_{\nu x}^r = \frac{1}{2\pi}\left(\sum_{\mu=1}^{N} \Gamma_{\Sigma\mu}^r \vartheta_{\mu\nu x} + \sum_{i=1}^{K} \delta_i \vartheta_{i\nu x} \right), \tag{5}$$

$$w_{\nu y}^r = \frac{1}{2\pi}\left(\sum_{\mu=1}^{N} \Gamma_{\Sigma\mu} \vartheta_{\mu\nu y} + \sum_{i=1}^{K} \delta_i \vartheta_{i\nu y} \right), \tag{6}$$

where $\vartheta_{\mu\nu x}$, $\vartheta_{\mu\nu y}$, $\vartheta_{i\nu x}$, $\vartheta_{i\nu y}$ are the influence functions in the control point ν from the integrated vortices μ и i of unit strength.

Using the tangency condition at all airfoil control points and the Thomson theorem on circulation invariance inside a closed contour enclosing the airfoil and its wake, the system of linear algebraic equations in unknown circulations of the integrated vortices located on the airfoil contour for the design instant of time r was written as:

$$\sum_{\mu=1}^{N} \Gamma_{\Sigma\mu}^r \left(\vartheta_{\mu\nu y} n_{\nu x} - \vartheta_{\mu\nu x} n_{\nu y} \right) + C = -2\pi \left[\; n_{\nu x} \left(\vartheta_{0y}^r + \vartheta_{0\varphi y}^r \right) - n_{\nu y} \left(\vartheta_{0x}^r + \vartheta_{0\varphi x}^r \right) - \right.$$

$$\left. - \sum_{i=1}^{K} \delta_i \left(\vartheta_{i\nu y} n_{\nu x} - \vartheta_{i\nu x} n_{\nu x} \right) \right], \tag{7}$$

$$\sum_{\mu=1}^{N} \Gamma_{\Sigma\mu}^r = F - \sum_{i=1}^{K} \delta_i \,, \nu = 1,2,...,N \,,$$

where F is the constant defined by initial conditions. The overdetermination of this system of equations was eliminated by introducing the regularizing variable C.

Upon solving the system of equations (7) and determining the circulations of integrated discrete vortices, the limiting values of the flow speed relative to the airfoil surface at the point ν were determined in the form:

$$w_{0\nu} = \left[\frac{1}{2\pi} \left(\sum_{\mu=1}^{N} \Gamma_{\Sigma\mu} \vartheta_{\mu\nu x} + \sum_{i=1}^{K} \delta_i \vartheta_{i\nu x} \right) + \vartheta_{0x} + \vartheta_{0\varphi x} \right] n_{\nu x} +$$

$$+ \left[\frac{1}{2\pi} \left(\sum_{\mu=1}^{N} \Gamma_{\Sigma\mu} \vartheta_{\mu\nu y} + \sum_{i=1}^{K} \delta_i \vartheta_{i\nu y} \right) + \vartheta_{0y} + \vartheta_{0\varphi y} \right] n_{\nu y} + \frac{\gamma_\nu}{2}, \tag{8}$$

where γ_ν is the dimensionless strength of the integrated vortex layer at the point ν being considered.

The flow parameters in the viscous region were determined by numerical integration of the system of differential equations for the unsteady boundary layer. For a laminar boundary layer this system has the form [6]:

$$\frac{\partial u}{\partial x}+\frac{\partial \vartheta}{\partial y}=0,$$

$$\frac{\partial u}{\partial t}+u\frac{\partial u}{\partial x}+\vartheta\frac{\partial u}{\partial y}=-\frac{1}{\rho}\frac{\partial p}{\partial x}+\vartheta\frac{\partial^2 u}{\partial y^2}, \qquad (9)$$

where u and ϑ are the air velocity components tangential and normal to the airfoil surface, x and y are the curvilinear coordinates in the boundary layer.

The second equation of system (9) for the turbulent boundary layer has the following form [7]:

$$\frac{\partial u}{\partial t}+u\frac{\partial u}{\partial x}+\vartheta\frac{\partial u}{\partial y}=\frac{\partial W}{\partial t}+W\frac{\partial W}{\partial x}+\frac{1}{\rho}\frac{\partial \tau^*}{\partial y}\quad , \qquad (10)$$

where τ^* is the shear stress.

For closure of the boundary layer equations, the van Driest-Klebanoff semiempirical two-layer eddy viscosity turbulence model based on generalized experimental data was used [1]. In so doing, for the internal boundary layer region the model based on Prandtl's mixing length concept was used and for the external region – the hypothesis of eddy viscosity constancy with accounting for Klebanoff's intermittency factor.

The finite-difference approximation for the continuity equation and for the fluid motion equation was made according to the 4-point and to the implicit 12-point computational schemes, respectively. In solution, the following commonly adopted conditions were used:

$$u(x,t)=0,\vartheta(x,t)=0 \quad \text{at } y=0,$$
$$u(x,t)\to W(x,t) \quad \text{at } y\to\delta, \qquad (11)$$

where δ is the boundary layer thickness. When specifying the initial velocity profiles at the boundary layer station, the exact solution of the Navier-Stokes equations in the vicinity of the stagnation point was employed.

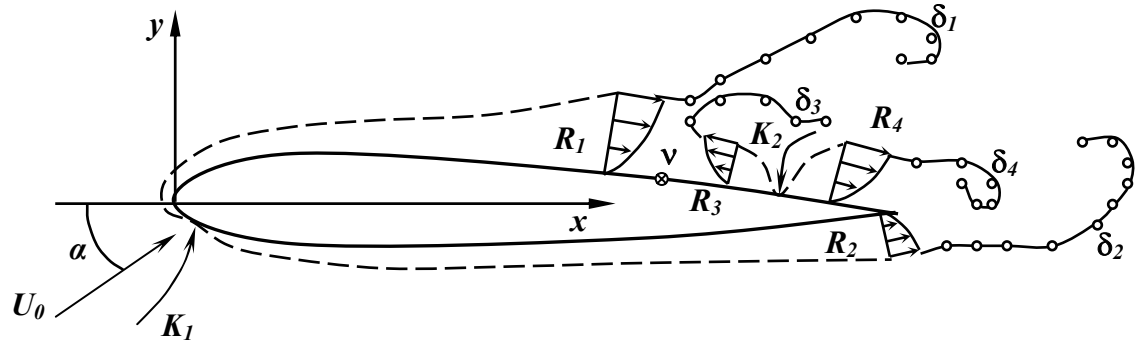

Figure 2. Computational scheme of separated flow around an airfoil

The boundary layer was calculated in the region from the point (K) (Fig.2) to the separation point (R) where either the surface friction became extremely small, that is, $\partial u/\partial y \to 0$, or the iteration process of solving the boundary layer equations became divergent. An important distinctive feature of the present model of separated flow is taking account of the boundary

layer in the reversed flow region. The number of stagnation points and separation points was not postulated and was determined in the course of calculations.

The wake behind the airfoil was modeled by free vortices whose strength was defined by the boundary layer vorticity at the flow separation points. The direction and speed of motion of each newly emanating free discrete vortex were defined by the flow velocity at the boundary layer station whereupon they moved together with the flow retaining their strengths.

The aerodynamic load on the airfoil section was determined at each time step r with the aid of the Cauchy-Lagrange integral. In so doing, the pressure coefficient $Cp\nu$ at the control point ν was determined as follows [2]:

$$Cp\nu = u_{0\nu}^2 - w_{0\nu}^2 - 2\frac{\partial\varphi}{\partial t}, \tag{12}$$

where the value of $\frac{\partial\varphi}{\partial t}$ was taken in the movable airfoil-fixed coordinate system. By integrating along the airfoil contour , the pressure coefficient Cp and friction factor τ_w as well as the coefficients of normal and longitudinal forces were calculated from the formulas:

$$C_y = -\oint \left[Cp\cos(n,y) + \tau_w \cos(n,x)\right]dS, \tag{13}$$

$$C_x = \oint \left[\tau_w \cos(n,y) - Cp\cos(n,x)\right]dS, \tag{14}$$

where S is the dimensionless curvilinear coordinate measured along the airfoil contour. The coefficient of pitching moment relative to the airfoil leading edge was calculated from the formula:

$$m_Z = -\oint\left\{x\left[C_p\cos(n,y) + \tau_W\cos(n,x)\right] - y\left[C_p\cos(n,x) - \tau_W\cos(n,y)\right]\right\}dS. \tag{15}$$

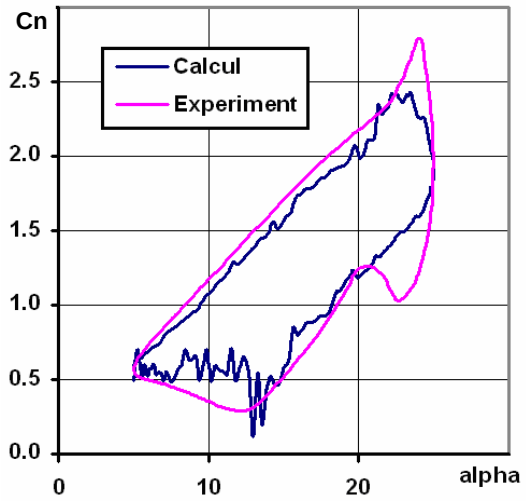

Figure 3. Plot of normal force coefficient as a function of angle of attack of the NACA 0012 airfoil

Systematic calculations were performed aimed at substantiation of the reliability of the computational model. [8]. By way of example (Fig. 3), the computed normal coefficient for the NACA 0012 airfoil was compared to the experimental data obtained by L. W. Carr [9]. The airfoil angle of attack varied according to the harmonic law

$$\alpha = 15^0 + 10^0 \sin 0{,}3\tau,$$

with the Reynolds number Re = $4\cdot10^6$.

2. SIMULATION RESULTS

2.1 Flow about an airfoil at fixed angle of attack

The simulation of the flow about the NACA 23012 airfoil using the above described model has shown that at small angles of attack the flow is attached. The boundary layer separation points on the upper and lower surfaces of the airfoil were situated near its trailing edge. As the angle of attack α increases, the load on the airfoil increases too, (Fig. 4), and as evident from Fig. 5, the curve $C_L\ (\alpha)$ remains linear up to $\alpha = 8^0$.

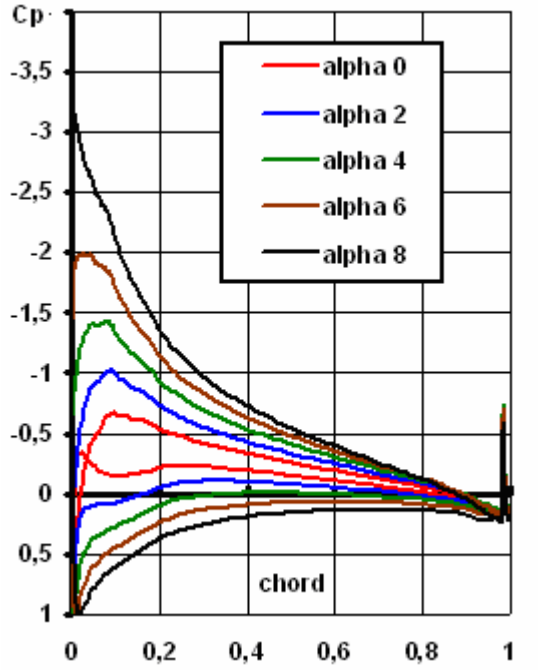

Figure 4. Airfoil section loading in the case of attached flow

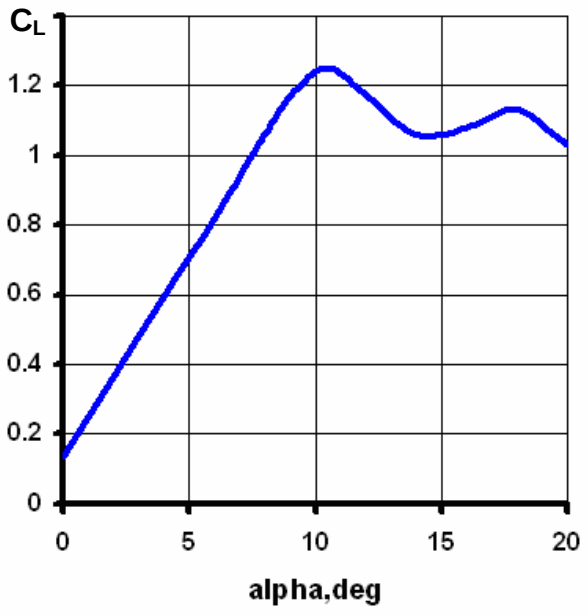

Figure 5. Airfoil lift coefficient versus angle of attack curve

Beginning from α=8,5^0, the boundary layer separation point on the upper surface moves upstream. Figure 6. shows the vortex layout of the airfoil NACA 23012 and the position of the separation point x_S (x_S /c is the relative separation point coordinate). Figure 7 illustrates the character of changes of the separation point location on the upper surface of the airfoil at different angles of attack.

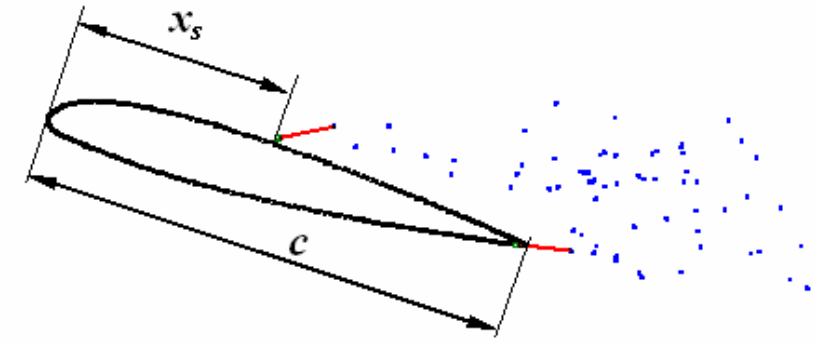

Figure 6. Vortex representation of the NACA 23012 airfoil. X_s – flow separation point coordinate; c –chord

The angle of attack range 8.5^0 to 11^0 can conditionally be defined as a transition from attached to developed separated flow. Both in the transient and separated flow regimes the location of the separation point as well as the instantaneous value of aerodynamic load vary with time

(Fig. 7). Figure 8 shows the instantaneous values of pressure coefficient on the airfoil, Fig. 5 shows the time-averaged values of the airfoil lift coefficient. The Reynolds number in these calculations was taken to be $6 \cdot 10^6$.

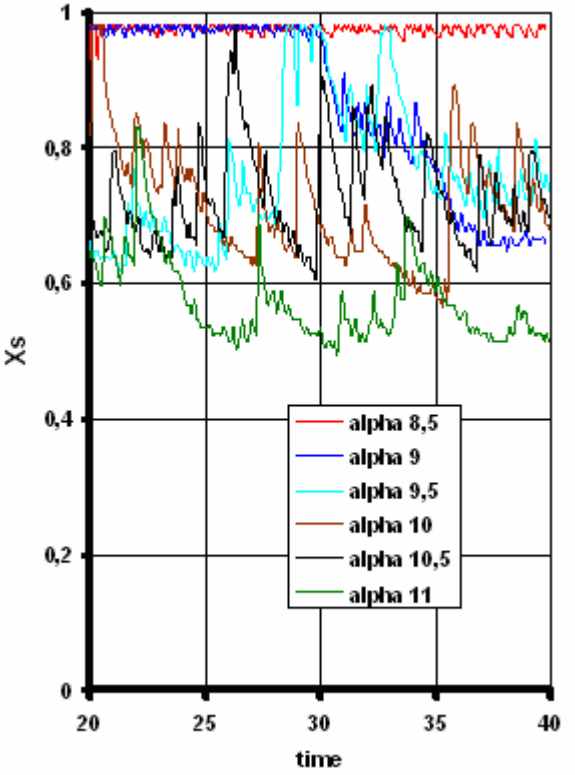

Figure 7. Temporal variation of the flow separation location in the transient flow regime of the NACA 23012 airfoil

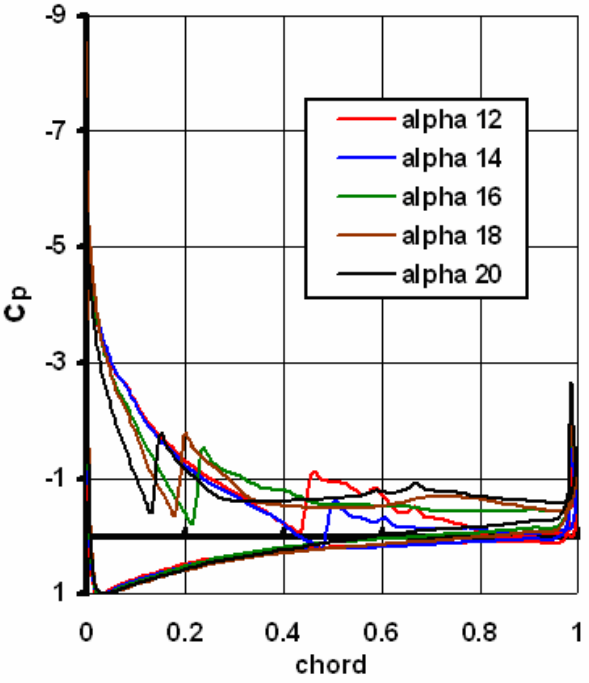

Figure 8. Airfoil section loading in the case of separated flow

2.2 Flow about an oscillating airfoil

When an flow-immersed airfoil has unsteady kinematic parameters, as for example in the case of its angle of attack varying according to a harmonic law, the character of variation of aerodynamic characteristics is known to considerably differ from the case of fixed angle of attack. To estimate the unsteadiness effect, the flow about a representative airfoil oscillating according to the law $\alpha = \alpha_0 - \Delta\alpha \cos \mathrm{Sh}\, t$ was numerically simulated.

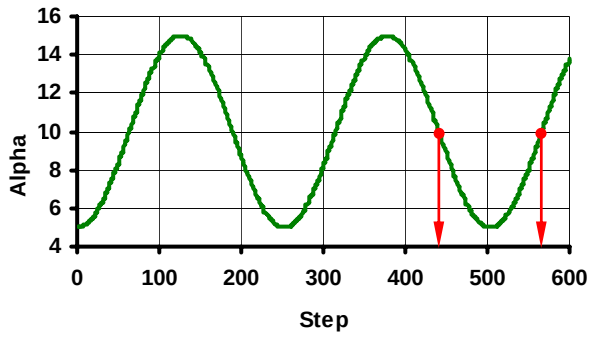

Figure 9. Time variation of the airfoil angle of attack according to the law $\alpha = \alpha_0 - \Delta\alpha \cos \mathrm{Sht}$ ($\alpha_0=10^0$; $\Delta\alpha=5^0$; Sh=0.25)

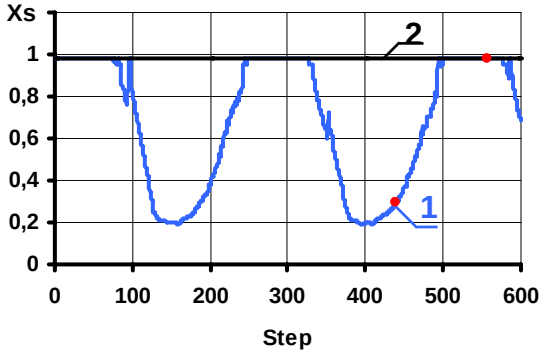

Figure 10. Separation point locations on the upper (1) and lower (2) airfoil surfaces

In the computations, the mean angle of attack was α_0 =10°, amplitude $\Delta\alpha$ = 5°, dimensionless frequency (Strouhal number) Sh = $2\pi f \cdot c/V$ = 0,25 (here f is the oscillation frequency, c is the airfoil chord, V is the flow speed). For this case, the temporal (depending on computation step) angle of attack variations are shown in Fig. 9, so that at some its values flow separation occurred. It is notable that both the 440th and 566th computation steps corresponded to one and the same angle of attack α =10° while at the 440th step the angle of attack was decreasing and at the 566th step it was increasing.

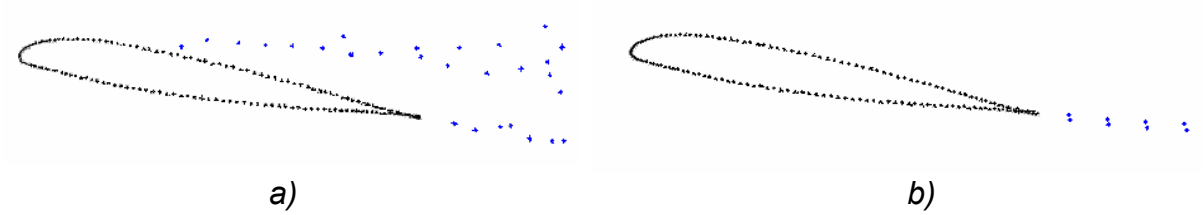

Figure 11. Vortex structure of the wake behind the airfoil at an instantaneous angle of attack $\alpha=10^0$ for the 440th (a) and 566th (b) computation steps

When at α_0 = 10° (440th computation step) the airfoil moved for decreasing, the separated flow covered most of the airfoil upper surface in contrast to the motion for increasing angle of attack (Fig. 10). The corresponding vortex structures confirm this (Fig. 11). In the normal force coefficient Cn versus α curve (Fig. 12), the instantaneous value α = 10° on the lower branch corresponds to the airfoil motion for decreasing angle of attack (440th computation step) and on the upper branch – for increasing angle of attack (566th computation step). In this case (α_0 = 10°) the difference in Cn values is large.

Figure 12. Normal force coefficient versus angle of attack curve for the harmonically oscillating airfoil at Sh=0.25

Of interest is the estimation of the Sh effect on the variation of aerodynamic characteristics with angle of attack when the airfoil oscillates harmonically. For this purpose, the flow about a helicopter airfoil was simulated with angle of attack oscillating according to the law $\alpha = 12.5^0 - 5^0 \cos \mathrm{Sh}\, t$ and the Strouhal number varying from Sh = 0,124 to Sh = 0,71.

The plots shown in Fig. 13. give the computed normal force coefficient as a function of angle of attack for different Sh values. The analysis of the investigation results has shown that with increasing the dimensionless airfoil oscillation frequency the area of the "loop" formed by the *Cn(α)* graph decreases. At Sh = 0,604 and Sh = 0,71 self - crossing "loops" form.

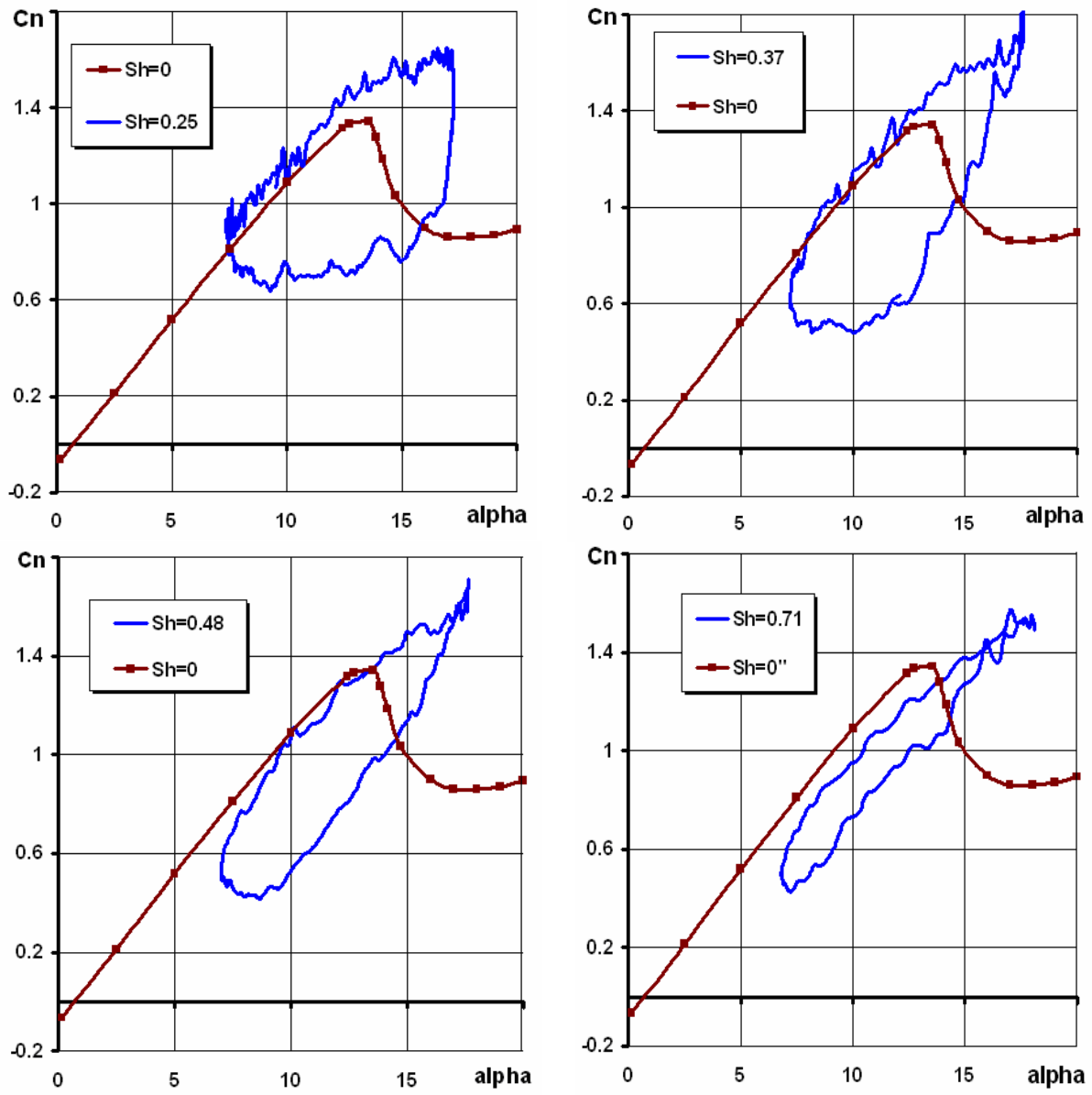

Figure 13. Strouhal number effect on the character of the curve Cn(α) for a harmonically oscillating helicopter blade airfoil

CONCLUSIONS

The mathematical model has been developed allowing the unsteady flow about helicopter blade airfoils to be simulated including the dynamic stall.

The model features a cost-effective computational scheme, which predetermines its deserving position in the hierarchy of mathematical models differing in accuracy and complexity.

REFERENCES

[1] S.M. Belotserkovsky, V.N. Kotovsky, M.I. Nisht, and R.M. Fedorov, *"Two-dimensional separated flows"*, CRC Press, Inc, 1993.

[2] S.M. Belotserkovsky and M.I. Nisht, *"Separated and nonseparated perfect fluid flow past thin airfoils"*, Nauka, Moscow, 1978.

[3] I.Yu. Brailovskaya and L.A. Chudov, *"Solvimg the boundary layer by the finite difference method"*, Computational Methods and Programming. Moscow State University Press, Vyp. 1, 1962.

[4] B.N.Yuryev, *"Aerodynamic calculation of helicopters"*, Oborongiz, Moscow, 1956.

[5] V.A. Anikin, and B.S. Kritsky, *"Multilevel mathematical model of rotorcraft aerodynamics"*, Proceedings of the 27th European Rotorcraft Forum, Moscow, Russia, 2001.

[6] H. Schlishting, *"Boundary Layer Theory"*, Nauka, Moscow, 1974.

[7] D.P. Telionis and D.Th. Tsahalis, *"Unsteady turbulent boundary layers and separation"*,AIAA Pap., Vol. 27, 1975.

[8] V.A. Anikin, O.V. Gerasimov, D.S. Kolomensky, E.B. Shumilina, B.S. Kritsky and G.G. Sudakov, *"Unsteady flow modeling and aerodynamics characteristics of helicopters airfoils"*, Proceedings of the 7th Annual Forum of the Russian Helicopter Society, March 2006.

[9] L.M. Carr, *"Progress in Analysis and Prediction of Dynamic Stall"*, J. of Aircraft. No.1, 1988.